Fluid-Structure-Acoustic Interaction of a simplified Towed Sonar Array System

Florian Wachter, Stefan Becker

Institute of Process Machinery and Systems Engineering, 91058 Erlangen, Germany, Email: wa@ipat.uni-erlangen.de

Introduction

Flow induced noise from the turbulent boundary layer that develops around a towed sonar array due to its relative motion through water significantly affects the quality of collected data. Understanding the fundamental mechanism of the self-noise generation is valuable for the improvement of signal-to-noise ratio and the development of new towed arrays [1].

Towed sonar arrays or streamers are utilized as underwater sound receivers. They are designed as long thin circular cylinders with hydrophones usually embedded in a highly viscous fluid in its centre line (see Fig. 1). These arrays typically have a large ratio of length to radius, in the order of 10^5. Due to this ratio, an axisymmetrical turbulent boundary layer (ATBL) develops around the cylindrical geometry that has a turbulent boundary layer thickness δ larger than the cylinder radius a ($\delta/a > 1$). Such an ATBL is visualized in Fig. 2 from a tow experiment [2].

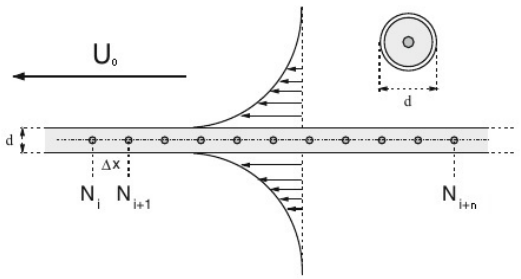

Figure 1: Sketch of a towed sonar array that illustrates the solid tube jacket and the hydrophones embedded in a highly viscous fluid in the centre line. Adopted from [3].

Figure 2: Photography of a turbulent boundary layer surrounding a streamer array - visualized by a single hole dye release, from [2].

In flows where $\delta/a > 1$, curvature effects become significant and lead to changes in the turbulent boundary layer (TBL), especially on mean velocity profiles, and turbulent fluctuations, causing higher skin-friction coefficients and different characteristics of wall-pressure fluctuations compared to the planar case (TBL of a flat plate or channel flow) [4][5][6][7]. These special features of the ATBL are relevant for the sonar array design because the performance of these devices is usually limited by the noise generated by the turbulent fluctuations around the surface of the streamer. Therefore, in our work we implement simulations that reproduce the fluid-structure-acoustic interaction for a simplified sonar array geometry to gain more insight into the governing generation mechanism of the TBL induced noise. Main sound sources like the turbulent wall pressure fluctuations on the cylinder surface and the acoustic source field around the array are assessed. In the following, the approach and the first results are presented.

Method and Setup

Given the discrepancy in the characteristic scales of the flow field and that of the sound field, it is common to use a hybrid approach and separate the computation of both problems [8]. Therefore, in the first step, the flow field is computed via a finite volume method and a large-eddy simulation in incompressible formulation using the open-source code OpenFOAM. As a sub-grid scale model, the WALE [9] formulation is used. The resulting turbulent wall pressure fluctuations and the acoustic source terms are then used as input data for the second step, a strong coupled mechanic-acoustic simulation. This resembles a one-way coupling between flow and mechanic computation and a two-way coupling between the mechanic and acoustic computation. The latter is realized with a finite element approach using the scientific code CFS++ [10].

The simulation domain and numerical grid of the flow computation is sketched in Fig. 3. The far-field boundary (f) radius is 30 times the radius of the cylinder (c) which resembles the streamer jacket. The domain length is 10 times the cylinder radius. To realize an axial flow over a long thin cylinder, periodic boundary conditions are applied in streamwise direction. The numerical grid has about $18{\cdot}10^6$ cells and the radius based Reynolds number Re_a is about 10^4.

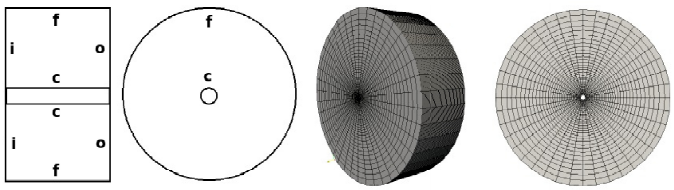

Figure 3: Sketch of the flow simulation domain in sectional side and frontal view - indicating inlet i, outlet o, far-field boundary f and cylinder wall c (left). Sketch of the numerical grid (right). The grid resolution is reduced for lucidity.

Two domains are at least required for the mechanic-

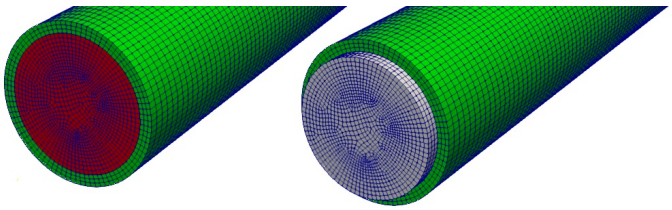

Figure 4: Sketch of the mechanic-acoustic simulation domain for computations with turbulent wall pressure fluctuations as input quantity. The left illustration shows the simulation domain with and the right one without the absorbing PML region.

acoustic simulation where turbulent wall pressure fluctuations on the cylinder surface are used as input quantity. In Fig. 4, the solid domain is indicated in green while the acoustic region is represented in red. The absorbing boundary regions are highlighted in grey where a perfectly matched layer method (PML) [11] is used.

Because no material data of a towed sonar array is available, materials and their parameters are assumed for the first simulations. For the solid jacket, a thermoplastic polyurethane was assumed with a density of $1.12 \cdot 10^3\ kg/m^3$, a Young's modulus of $18.7 \cdot 10^6\ Pa$ and a Poisson number of 0.48. For the fluid filling in the acoustic domain, water was used with a density of $0.997 \cdot 10^3\ kg/m^3$ and a compression modulus of $2.08 \cdot 10^9\ Pa$. Additionally, a mineral oil with a density of $0.83 \cdot 10^3\ kg/m^3$ and a compression modulus of $1.6 \cdot 10^9\ Pa$ was conducted for comparison. Five hydrophones (A-E) are positioned within the centre line of the acoustic domain. Each hydrophone is represented by seven point probes to take the radius of the transducer into account (positions: centre, north, south, west, east, top, bottom).

The dynamic behaviour of the mechanic system is defined by Navier's equation while the acoustic wave propagation is described by the linear acoustic wave equation. The mechanic-acoustic coupling is realized with Eq. 1 and Eq. 2. The first equation states that the wall-normal component of the mechanical surface velocity $\mathbf{v}_s$ is equal to the wall-normal component of the acoustic particle velocity $\mathbf{v}_a$. The second one is derived from the first one and describes the relation between the solid surface displacement $\mathbf{s}$ and the acoustic pressure p_a.

$$\mathbf{n} \cdot (\mathbf{v}_s - \mathbf{v}_a) = 0 \tag{1}$$

$$\mathbf{n} \cdot \frac{\partial^2 \mathbf{s}}{\partial t^2} = -\frac{1}{\rho_0} \frac{\partial p_a}{\partial \mathbf{n}} \tag{2}$$

For the mechanic-acoustic simulation with acoustic source terms as input quantity, the material parameters remain unaltered. However, the simulation domain is constructed differently. To interpolate the acoustic source terms that are located in close proximity around the cylinder jacket, an additional acoustic region is appended. The overall simulation domain is illustrated in Fig. 5 and exhibits the water or oil filling (red), the solid jacket (green), the additional water surrounding (purple) and the absorbing PML region (grey).

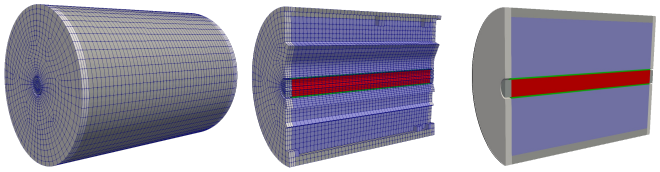

Figure 5: Sketch of the mechanic-acoustic simulation domain for computations with acoustic source terms as input quantity. The grid resolution is reduced for lucidity.

One of the applied acoustic source term formulation is Lighthill's inhomogeneous wave equation for the fluctuating pressure p' (Eq. 3). The double divergence of the simplified Lighthill stress tensor $T_{ij} \approx \rho_0 u_i u_j$, which is valid for incompressible flows, is used here as the acoustic source term. Where ρ_0 is the density and $u_i u_j$ the correlation of the instantaneous velocity components of the flow. Another utilized analogy is the "perturbed convective wave equation" (PCWE) which is stated in Eq. 4. Here, the source term is the substantial derivative of the incompressible flow pressure Dp^{ic}/Dt. The relationship between the acoustic scalar potential ψ_a and the acoustic pressure p_a is defined by $p_a = D\psi_a/Dt$ (for details see [11]). The speed of sound is abbreviated by c_0.

$$\frac{1}{c_0^2} \frac{\partial^2 p'}{\partial t^2} - \frac{\partial^2 p'}{\partial x_i^2} = \frac{\partial^2 T_{ij}}{\partial x_i \partial x_j} \tag{3}$$

$$\frac{1}{c_0^2} \frac{D^2 \psi_a}{Dt^2} - \nabla \psi_a = \frac{1}{\rho_0 c_0^2} \frac{Dp_{ic}}{Dt} \tag{4}$$

The main idea of the simulations using the acoustic analogies is to utilize the source terms as sound sources and compute the sound propagation and the resulting excitation of the solid to finally see the impact on the resultant spectrum. Since the Lighthill formulation is known to be unable to separate acoustic and hydrodynamic pressure fluctuations in the near-field of the source locations, the PCWE formulation was included in the investigations. It delivers an acoustic field that is free from dynamic flow disturbances [11].

Flow Simulation Results

To validate the results of the flow simulation, the work of [12], [13] and [14] was considered. The simulations show ratios of $\delta/a \approx 12$. In the literature, experiments under laboratory conditions and numerical work state δ/a values between four and nine. For towing tests under realistic conditions, ratios of $\delta/a \approx$ 10-12 are known [1]. The resulting dimensionless radius $a^+ = au_\tau/\nu$ shows values around 450 what fits quite well to the literature data. Also, the evaluated skin-friction coefficient $C_f \approx 0.003$ agrees with validation data for similar Re_a.

Profiles of the mean velocity (Fig. 6), the Reynolds stress (Fig. 7) and the root-mean-square pressure fluctuations (Fig. 8) are presented, exemplarily, to demonstrate that the flow simulation delivers reliable data. The coloured lines indicate the simulation results for different configurations regarding pressure-velocity coupling and realization of periodic boundary conditions. The black lines and symbols refer to data from literature.

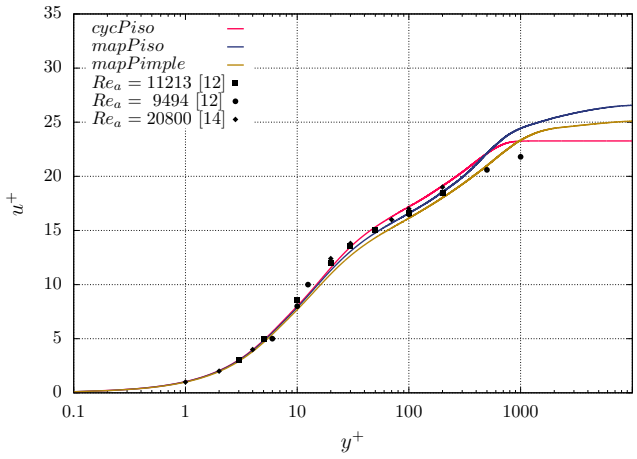

Figure 6: Mean velocity profile as function of the dimensionless wall-distance.

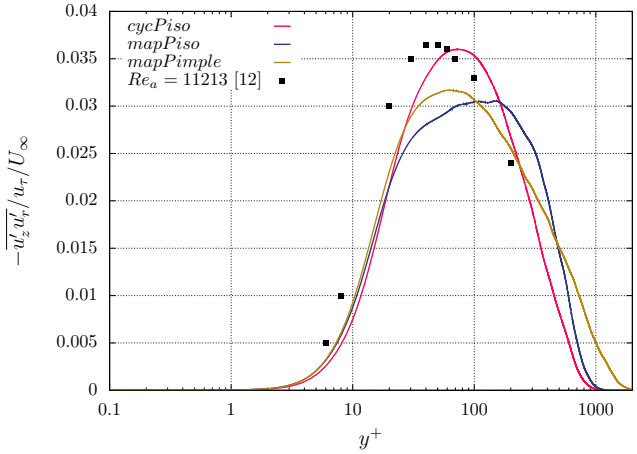

Figure 7: Reynolds stress profiles normalized by friction and freestream velocity as function of the dimensionless wall-distance.

The mean velocity profiles from the simulations show a good overall agreement with the validation data. For the Reynolds stresses, we see differences between the configurations in which the "*cycPiso*" settings comes closest to the literature values. The pressure fluctuations are slightly over-predicted in comparison to the reference data. Turbulent flow structures and vortices visualized by the iso-surfaces of the λ_2-criterion (not shown here) exhibit a similar structure as presented in [15]. The results of the "*cycPiso*" simulation configuration are used for the subsequent mechanic-acoustic computations.

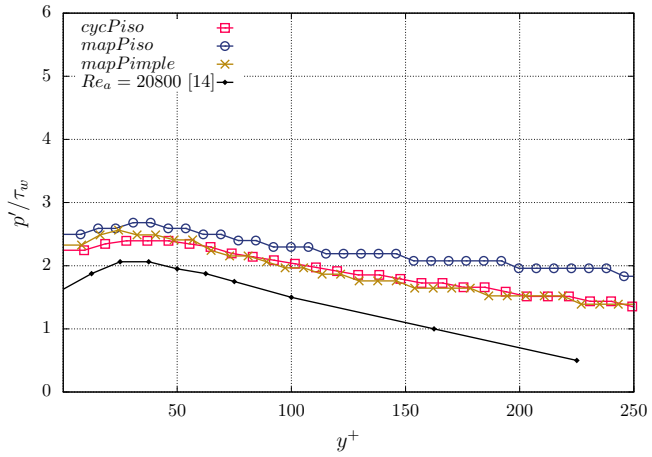

Figure 8: Root-mean-square pressure fluctuations normalized by wall shear stress as function of the dimensionless wall-distance.

Mechanic-Acoustic Simulation Results

The outcome of the mechanic-acoustic simulations with acoustic source term input are not presented within this report. The focus of this section lies on the findings of the computations where the turbulent pressure fluctuations on the cylinder surface are used as input quantity.

For the evaluation of the mechanic-acoustic simulation, all time signals from the seven point probes are averaged for each hydrophone. The resulting power spectral density (PSD) for all five hydrophones (A-E) is presented in Fig. 9.

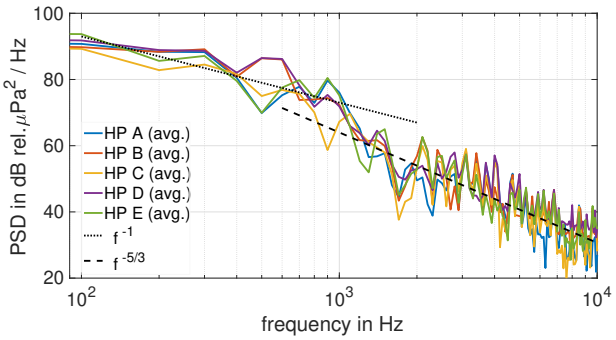

Figure 9: Power spectral density of the averaged time signal for each hydrophone (HP) A to E. Additionally, f^{-1} and $f^{-5/3}$ decays are indicated.

A signal length of 0.02 s and a sample rate of 100 kHz was available from the first simulation. Three Hamming windows were used with 50% overlap leading to a frequency resolution of 100 Hz. A closer analysis of the spectra reveals a f^{-1} decay for 100 Hz to 1000 Hz and a $f^{-5/3}$ decay for higher frequencies. This coincides with the statement from [16] reporting a universal power law decay of ω^{-1} (angular frequency) for the spectrum of wall pressure fluctuations in TBL for intermediate frequencies. Also, the decay of $f^{-5/3}$ shows the same slope as the energy spectrum of turbulence in the so called inertial sub-range. No difference was observed in the out-

come between the mineral oil and the water filling in the acoustic domain.

Summary

The fluid-structure-acoustic interaction (FSAI) simulation is a promising method to investigate and understand the principal generation mechanism of turbulent boundary layer induced self-noise of towed sonar array systems. A work-flow was established to realize FSAI computations for a simplified streamer geometry where a one-way coupling was used between the flow and structural dynamics. Between the structural dynamics and the acoustics, a two-way coupling was applied.

The flow simulations with radius based Reynolds numbers Re_a around 10^4 show good agreement with literature data. The results of the mechanic-acoustic simulation are presented where turbulent wall pressure fluctuations from the flow computations are used as input quantity. No mentionable impact was observable in the results when using a mineral oil or water as filling medium. The cognizable f^{-1} and $f^{-5/3}$ decay in the power spectral densities could be interrelated to universal decay laws for wall pressure fluctuations in turbulent boundary layer flows [16] and the energy cascade of turbulence. Results from the mechanic-acoustic simulation where acoustic source terms are used as input data are not shown within this report. However, the comparison of the outcomes of these two approaches may reveal some insight into the generation mechanism of flow noise regarding the separated sound sources, namely, turbulent wall pressure fluctuations on the cylinder surface and the acoustic source terms around the cylinder. Such an analysis will be presented in a prospective report.

References

[1] Elboth T., Lilja D., Reif B.A., Andreassen Ø., Investigation of flow and flow noise around a seismic streamer cable. Geophysics, 75(1), Q1-Q9, 2010.

[2] Elboth T., Wasberg C.E., Helgeland A., Andreassen Ø., Reif B.A.P., Flow noise simulations around a cylinder. MekIT'09 Fifth national conference on Computational Mechanics. Tapir Academic Press, 2009.

[3] Abshagen J., Möser M. (Ed.), Wasserschallmessungen. Springer Vieweg, Berlin, Heidelberg, 2018.

[4] Lueptow R.M., Turbulent boundary layer on a cylinder in axial flow. AIAA journal, 28(10):1705–1706, 1990.

[5] Monte S., Sagaut P., Gomez T., Analysis of turbulent skin friction generated in flow along a cylinder. Physics of Fluids, 23(6):065106, 2011.

[6] Neves J.C., Moin P., Moser R.D., Effects of convex transverse curvature on wall-bounded turbulence. Part 1. The velocity and vorticity. Journal of Fluid Mechanics, 272:349–382, 1994.

[7] Neves J.C., Moin P., Effects of convex transverse curvature on wall-bounded turbulence. Part 2. The pressure fluctuations. Journal of Fluid Mechanics, 272:383–406, 1994.

[8] Wagner C., Hüttl T., Sagaut P. (Eds.), Large-eddy simulation for acoustics, Vol. 20, Cambridge University Press, 2007.

[9] Ducros F., Nicoud F., Poinsot T., Wall-adapting local eddy-viscosity models for simulations in complex geometries. Numerical Methods for Fluid Dynamics VI, Oxford University Computing Laboratory, 1998. p.293-299.

[10] CFS++: Coupled Field Simulation Applied Mechatronics, Institute of Sensor Technology - University Erlangen, Technical Report, 2010.

[11] Kaltenbacher M., Numerical simulation of mechatronic sensors and actuators, Vol. 3, Springer Berlin, Heidelberg, 2015.

[12] Jordan S.A., Axisymmetric turbulent statistics of long slender circular cylinders. Physics of Fluids, 23(7):075105, 2011.

[13] Willmarth W.W, Winkel R.E, Sharma L.K., Bogar T.J., Axially symmetric turbulent boundary layers on cylinders: Mean velocity profiles and wall pressure fluctuations. Journal of Fluid Mechanics, 76(1):35–64, 1976.

[14] Woods M.J., Computation of axial and near-axial flow over a long circular cylinder. PhD thesis, Mechanical Engineering School, University Adelaide, Australia, 2006.

[15] Jordan S.A., Near-wall turbulent characteristics along very long thin circular cylinders. Journal of Fluids and Structures, 27(3):329–341, 2011.

[16] Camussi R., Noise sources in turbulent shear flows: Fundamentals and applications (Vol. 545), Springer Science and Business Media, 2013.